The Astrophysical Journal Letters, 960:L5 (7pp), 2024 January 1 https://doi.org/10.3847/2041-8213/ad1580

4FGL J1318.2+6754: A Long Orbital-period Redback Candidate

Jie Lin[1,2,3], Hailiang Chen[4,5], Bojun Wang[6], and Renxin Xu[1,2,3]
[1] State Key Laboratory of Nuclear Physics and Technology, Peking University, Beijing 100871, People's Republic of China; j.lin@pku.edu.cn
[2] Department of Astronomy, School of Physics, Peking University, Beijing 100871, People's Republic of China; r.x.xu@pku.edu.cn
[3] Kavli Institute for Astronomy and Astrophysics, Peking University, Beijing 100871, People's Republic of China
[4] Yunnan Observatories, Chinese Academy of Sciences, Kunming 650216, People's Republic of China
[5] International Centre of Supernovae, Yunnan Key Laboratory, Kunming 650216, People's Republic of China
[6] National Astronomical Observatory, Chinse Academy of Sciences, Beijing 100101, People's Republic of China
Received 2023 August 22; revised 2023 November 17; accepted 2023 December 13; published 2024 January 3

Abstract

By combining the Fermi catalog and the single-lined spectroscopic binaries of Gaia Data Release 3 (DR3), we report a new candidate redback millisecond pulsar binary, which is recommended as a target for radio telescopes to detect pulsed signals. Using TESS data in the *T* band spanning over 4 yr, we find a period of ∼4.13 days, which is consistent with the radial velocity solution of the Gaia DR3 and optical spectroscopy from the LAMOST telescope. The light curve in the *T* band reveals periodic modulation of low amplitude that is a characteristic feature of the heating of the photosphere of a nondegenerate low-mass stellar companion by the pulsar wind. The nondegenerate companion is a bright ($G = 11.96$), slightly metal-poor ($[\mathrm{Fe/H}] = -0.55$), G-type main-sequence star ($T_{\mathrm{eff}} = 5891$ K; $\log g = 4.07$; $R = 1.356 R_{\odot}$). This orbital period of 4.13 days would be the longest one for known redback candidates, which could hardly be understood for its formation in the standard recycling scenario due to its large Roche-lobe radius (≫the radius of the G-type main-sequence star). It is proposed here that this candidate redback millisecond pulsar binary could be created via accretion-induced collapse of an oxygen–neon–magnesium white dwarf.

Unified Astronomy Thesaurus concepts: Neutron stars (1108)

1. Introduction

Spider pulsars are an interesting subclass of millisecond pulsars (MSPs), the so-called "redbacks" and "black widows." The former have nondegenerate 0.1–1 $M_{\odot}$ companions, while the latter have very low mass companions, $M_c \ll 0.1 M_{\odot}$ (Roberts 2013). The side of the companion star facing the pulsar is heated due to either high-energy photons from the shock or direct bombardment by pulsar wind particles (Bogdanov et al. 2011; Romani & Shaw 2011; Kong et al. 2012; Breton et al. 2013; Gentile et al. 2014; Burdge et al. 2022). The optical modulation can be dominated by the contrast on the companion's dayside with respect to their nightside. If the heating effect is small, the light curve will show the ellipsoidal modulation from the tidally distorted star. Studying spider systems can provide an opportunity to measure the mass of the hosted neutron star (NS), which is important for revealing the equation of state of supranuclear densities inside NSs (Romani et al. 2022).

The standard model for the formation of MSPs is the recycling scenario. In this scenario, MSPs are believed to be old NSs, formed via core-collapse supernovae (SNe) or electron capture supernovae (ECSNe), that have accreted material and angular momentum from their companion stars in a low-mass X-ray binaries (LMXBs; Alpar et al. 1982). There are redbacks, known as transitional millisecond pulsars (tMSPs), that show transitions between accretion-powered and rotation-powered pulsar states (Archibald et al. 2009; Papitto et al. 2013). tMSPs may be the evolutionary link between MSPs and LMXBs, supporting the recycling scenario (Archibald et al. 2009; Papitto et al. 2013). However, there are still many unanswered questions about details of the formation and evolution of the spider system (Chen et al. 2013; Benvenuto et al. 2014; Ablimit 2019).

Radial-velocity modulation in optical spectra is a promising method to uncover NSs that have a stellar companion (Yi et al. 2022; Yuan et al. 2022; Zheng et al. 2023; Lin et al. 2023). In addition, the Fermi Large Area Telescope has certain advantages in discovering spider pulsars. We proposed a method to search for spider pulsar candidates by combining the γ-ray source of Fermi and radial-velocity modulation of optical spectra in the epoch of large-scale spectroscopic surveys (e.g., LAMOST and Gaia; Cui et al. 2012; Gaia Collaboration et al. 2023). This method may help us to discovery more spider pulsars and some special spider pulsar candidates, which will provide an unprecedented opportunity to understand the spider system and measure the NS's mass.

In this Letter, we report a single-lined binary consisting of a G-type main-sequence star and an unseen object associated with the Fermi γ-ray source 4FGL J1318.2+6754, which is likely a binary in a long-period and low-inclination orbit around a neutron star. If the dark object is identified as an MSP, this may suggest that it was formed by accretion-induced collapse (AIC) of a white dwarf (WD). This Letter is organized as follows. The analysis and result are described in Section 2. The general discussion of the source is given in Section 3. Our conclusions are presented in Section 4.

2. Data Analysis

2.1. Searching for MSP Candidates with 4FGL-DR3/Gaia DR3

Gaia Data Release 3 (DR3) contains more than 181,000 orbital solutions for single-lined spectroscopic binaries (SB1s)

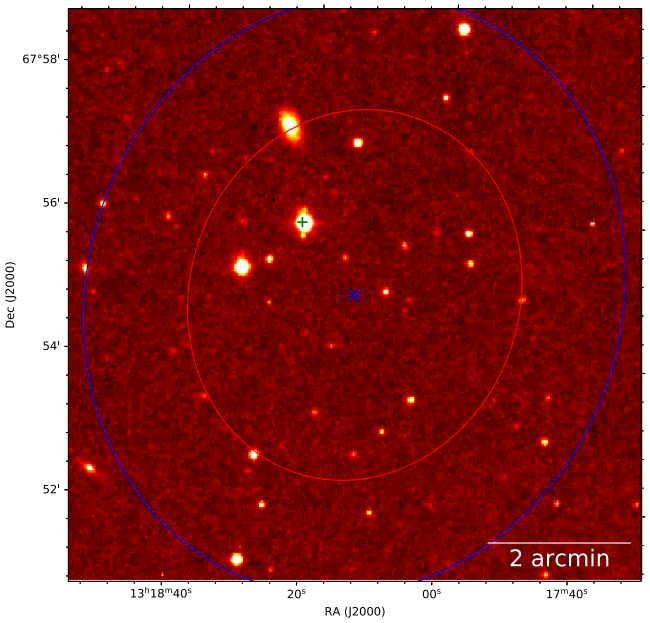

Figure 1. The Digitized Sky Survey (DSS) image of 4FGL J1318.2+6754. The red and blue ellipses show a 68% error ellipse and 95% error ellipse of the 4FGL catalog, respectively. The small pink plus is the position determined by the SB1 of Gaia DR3, which is located at a 95% confidence level of 4FGL J1318.2+6754.

that can be used to discover candidates with a black hole or neutron star companion (Gaia Collaboration et al. 2023). In addition, Data Release 3 of the fourth Fermi Large Area Telescope catalog provides >2000 unassociated γ-ray sources. In this project, we crossmatched the Gaia-DR3 SB1s and the 4FGL-DR3 and selected those with relatively large mass-functions in the radial-velocity (RV) solutions of Gaia DR3. One strong candidate was discovered with the optical source of Gaia DR3 located at R.A.(J2000) = $13^{\rm h}18^{\rm m}21\overset{\rm s}{.}65$ and decl. (J2000) = $+67°55'53\overset{''}{.}5$, inside the 95% error region of the γ-ray source 4FGL J1318.2+6754 (see Figure 1). In Gaia DR3, the source_id of J1318 is 1684686323263180160 with a bright ($G = 11.96$) solar-type star. Its DR3 parallax of $\omega_{\rm DR3} = 2.490610 \pm 0.012581375$ mas implies a distance of $d \sim 402$ pc. The RV solution of Gaia DR3 gives the orbital period ($P = 4.129265937434151 \pm 0.0005006378$ days), eccentricity ($e = 0.05 \pm 0.03$), semiamplitude ($K = 48.713 \pm 1.13\,{\rm km\,s^{-1}}$), and center-of-mass velocity ($\gamma = -14.95 \pm 0.762\,{\rm km\,s^{-1}}$), respectively. We can obtain the mass function $f(M) = PK^3(1-e^2)^{3/2}/2\pi G \sim 0.049 M_\odot$, where G is the gravitational constant. The Fermi γ-ray source 4FGL J1318.2+6754 was proposed to be associated with a blazar candidate of unknown type (Abdollahi et al. 2022). Its flux in the 0.1–100 GeV band is $(1.34 \pm 0.26) \times 10^{-12}\,{\rm erg\,cm^{-2}s^{-1}}$and its γ-ray spectrum can be fitted with a logParabola model (Abdollahi et al. 2022).

In this context, we have devoted some effort to investigating the nature of the counterpart of the secondary of 4FGL J1318.2+6754, namely J1318 with possible association with the γ-ray source. We find that the best location of the gamma-ray source is $1\overset{''}{.}25$ from the optical source of Gaia DR3, which was suggested as a potential counterpart. Using Gaia DR3 (Gaia Collaboration 2022), there are a total of 51 stars in the error box. Then, the surface number density of the star is $\rho_1 \approx 51/(50.26\,{\rm arcmin^2}) \approx 1.01/{\rm arcmin^2}$ in the error box, which means a low stellar density. In addition, we calculate probability of chance coincidence between γ-ray sources and the optical source of Gaia DR3. Here, we retrieved the SB1s, with R.A.(J2000) = 195°–205° and decl.(J2000) = 65°–75°, from Gaia DR3 (Gaia Collaboration et al. 2023), and we assume that the spatial distribution of SB1s is isotropic within a specific sky area. There are 56 SB1s in this area and the surface density of the SB1s is $\rho_2 \approx 56/(360000\,{\rm arcmin^2}) \approx 1.6 \times 10^{-4}/{\rm arcmin^2}$. We assume that the number of SB1s within the 95% error box satisfies the Poisson distribution. Therefore, the probability of chance coincidence is $P = \lambda^1 \exp(-\lambda)/1! = 1\%$, where $\lambda = \rho_2 S$ is the expected number of SB1s and S ($\sim$64 arcmin^2) is area of the 95% error box.

2.2. Optical Photometry

We then further cross-checked the candidate with the SIMBAD database and found that the optical source (TIC 232972548) was observed by TESS in Sectors 14, 15, 21, 22, 41, 48, and 49 from 2019 July to 2022 February. TIC 232972548[7] was observed with 600 and 1800 s cadences, respectively. We used the Lomb–Scargle method (Lomb 1976; Scargle 1982) to search for variability on the timescale of days in the TESS T-band light curve and found evident periodic signatures with $P = 4.137258763046017$ days (see Figure 2). The period of the TESS T-band light curve basically agrees well with the radial-velocity (RV) solutions of Gaia DR3, which suggests that the solutions of Gaia DR3 should be right. In addition, the light curve of the optical source is consistent with a redback MSP binary when its nondegenerate companion is significantly heated by the pulsar (Bogdanov et al. 2011; Romani & Shaw 2011; Kong et al. 2012; Breton et al. 2013; Gentile et al. 2014; Burdge et al. 2022).

Here, we also note that the light curve in Figure 2 changes significantly between different epochs. To see how the power of the peak at 4.13 days changes and if there is any obvious tidal deformability signal (at 0.5P), we compute separate Lomb–Scargle periodograms for each epoch (see Figure 3). Interestingly, the inferred maximum value of the Lomb–Scargle periodograms on 2020 January 21, 2021 July 24, 2022 January 28, and 2022 February 26 deviates slightly from the orbital period of the entire data set. These deviations may result from the presence of an extra peak (periodic signal) in the vicinity of the orbital period. Considering that these four epochs in Figure 2 show irregular and asymmetric optical light curves, the peak of the vicinity of the orbital period may be a starspot that traces stellar rotation (van Staden & Antoniadis 2016), which suggests the G-type star may be in asynchronous rotation. The separate Lomb–Scargle periodogram seems to suggest the presence of a tidal deformability signal in partial epochs. If the signal is indeed a tidal deformability signal, the first harmonic (at 0.25P) of the tidal deformability signal should be detected and the signal should be presented in all epochs. However, we do not find the presence of the first harmonic and the detection of the signal in all epochs. Therefore, the obvious signal at 0.5P likely may be the first harmonic of the orbital period in partial epochs. The lack of a tidal deformation signal implies a small filling factor, which is consistent with the filling factor inferred from the spectral energy distribution (SED).

[7] The data are available at the Mikulski Archive for Space Telescopes (MAST) at the Space Telescope Science Institute doi:10.17909/npw9-rn37.

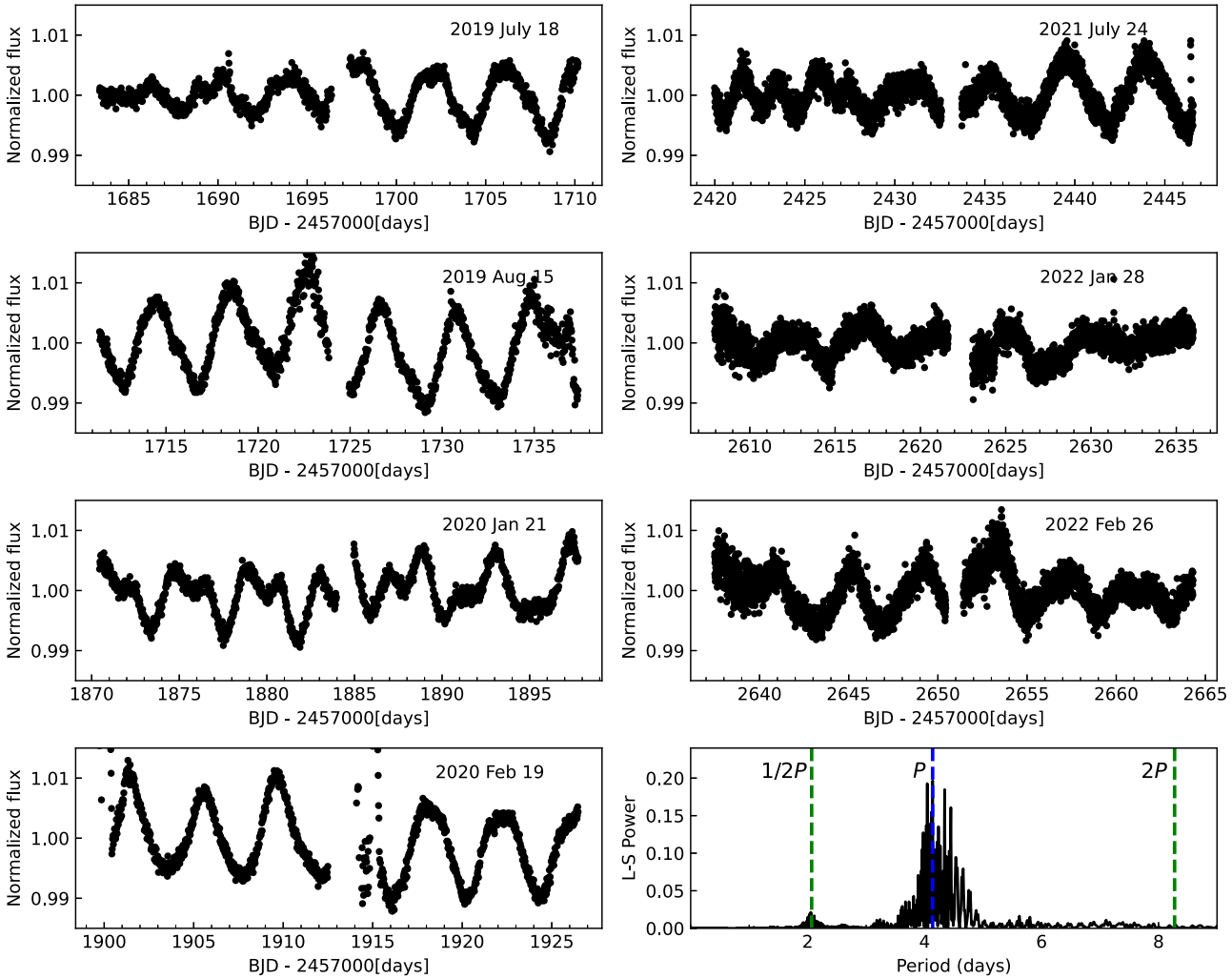

Figure 2. The TESS light curves for J1318 from 2019 July to 2022 February. The Lomb–Scargle periodogram of the entire data set for TESS, showing a clear peak around 4.13 days.

In order to verify the primary is a compact object, we retrieved photometry of the source in Gaia DR3 (G, $G_{\rm BP}$, and $G_{\rm RP}$), 2MASS (J, H, and $K_{\rm s}$), SDSS (u, g, r, i, and z), JOHNSON (B and V), WISE (W1 and W2), and TESS (T), and fit the SED with the spectral energy distribution Bayesian model averaging fitter (astroARIADNE[8]; Vines & Jenkins 2022). The SED fit yields $T_{\rm eff} = 5891.26^{+49.62}_{-52.40}$ K, $R = 1.356^{+0.013}_{-0.035}\,R_{\odot}$ by using the extinction value of $A_{\rm v} = 0$ derived from three-dimensional dust maps (Green et al. 2019), where $A_{\rm v}$ is the extinction measured in the V band. We find that the source is well fit by a single-star model (see Figure 4), which also suggests that the primary is likely a compact object.

2.3. Optical Spectroscopy

To further validate the orbit of Gaia DR3, we search for archival data by other telescopes. The source was observed by the LAMOST survey in 2019, which obtained four medium-resolution spectra of J1318 from the LAMOST archive data. The medium-resolution spectra have $R\sim7500$ and a limiting magnitude of about $G = 15$ mag (Zong et al. 2020). The blue arm of the medium-resolution spectra covers the range from 495 to 535 nm, and the red arm covers the range from 630 to 680 nm. We derived the barycentric velocity of each spectrum through the cross-correlation technique. In addition, the optical spectroscopy of LAMOST also presents a single-line binary (one visible star only). For four medium-resolution spectra, we use the spectra of the blue arms to measure RVs. The cross-correlation has been performed using the spectral template ($T_{\rm eff} = 5800$ K, $\log g = 4.44$, and $[{\rm Fe/H}] = 0$) calculated with the MARCS model (Gustafsson et al. 2008). The RV was obtained and we performed the Gaia SB1 solution fit to our radial-velocity data using the custom Markov Chain Monte Carlo sampler TheJoker (Price-Whelan et al. 2017; see Figure 5).

To derive the surface gravity and metallicity of the G-type star, we use the spectral synthesis codes iSpec (Blanco-Cuaresma et al. 2014; Blanco-Cuaresma 2019). iSpec generates synthetic spectra based on the SPECTRUM (Gray & Corbally 1994) and MARCS (Gustafsson et al. 2008) model atmospheres and outputs the best-fitting stellar parameters using a χ^2-minimization process. For the iSpec fits, we initially keep the surface temperature fixed at $T_{\rm eff} = 5891$ K from the result of the SED. These fits yield $\log g = 4.07 \pm 0.32$, $[{\rm Fe/H}] = -0.55 \pm 0.13$, and $[\alpha/{\rm Fe}] = 0.10 \pm 0.22$ (Figure 6). The temperature and radius measured from the SED to single-star

[8] https://github.com/jvines/astroARIADNE

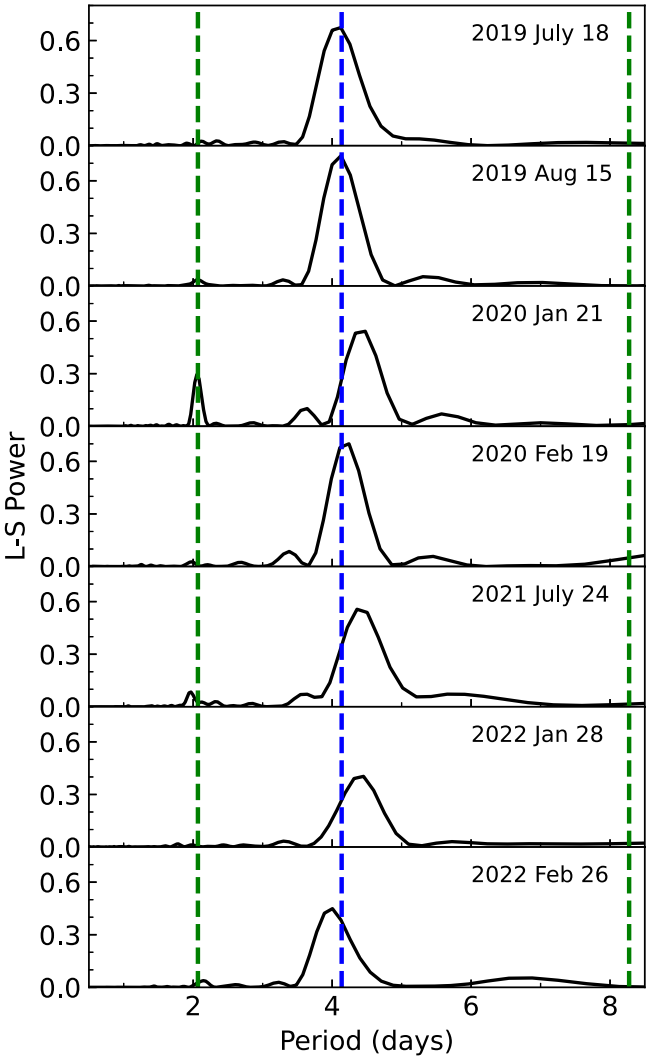

Figure 3. The Lomb–Scargle periodogram of the TESS light curve for different epochs. The dashed blue line is the orbital period obtained by he entire data set, while the dashed green line is the harmonic of the orbital period.

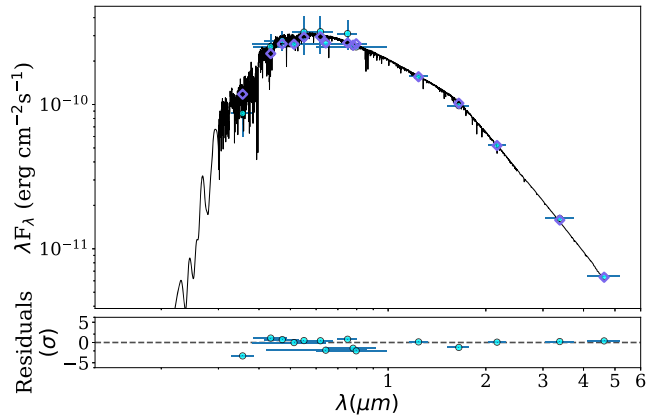

Figure 4. The best-fitting SED model for J1318 after fixing the extinction parameters $A_v = 0$. The black curve is the best-fitting model. The green pluses and circles are the retrieved photometric measures. The blue diamonds are synthetic photometry.

MIST evolutionary models with [Fe/H] = − 0.5 (Choi et al. 2016; Dotter 2016), suggesting a mass of $0.84 \pm 0.02 M_\odot$ and the star is evolved. The radius of the Roche lobe has

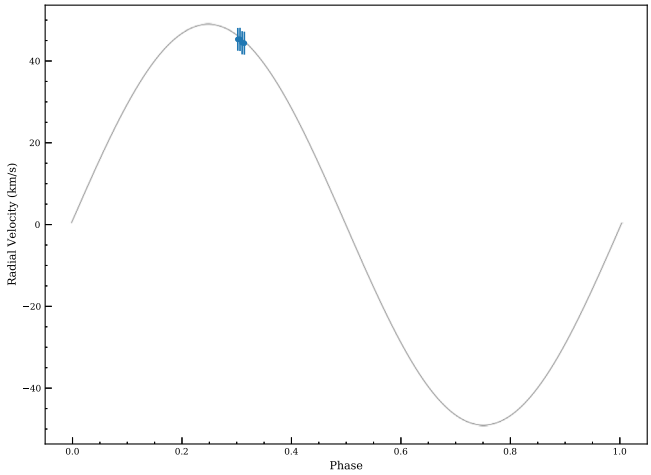

Figure 5. The observed radial velocities for J1318 as a function of the orbital phase obtained in four epochs from LAMOST, with the radial-velocity solution of Gaia DR3 plotted.

$R_L = (2M_2GP^2/81\pi^2)^{1/3} = 4.71R_\odot$, where P is the orbital period, and $M_2 = 0.84M_\odot$. The radius of the Roche lobe is far larger than the radius ($\sim 1.36R_\odot$) of the G-type star from the SED, which indicates a small filling factor of about 30%.

2.4. Constraints on the Inclination

We found a variable, single-lined optical source inside the 95% error ellipse of 4FGL J1318.2+6754. It resembles a redback pulsar with the optical modulation due to heating of the photosphere of a low-mass companion star by an MSP. Therefore, we speculated that it is an MSP binary candidate with a long-period orbit. We used the ELC code (Version 7; Orosz & Hauschildt 2000) to model the TESS light curves for J1318 in 2019 August because the heating light curves seem to be more symmetric compared to other epochs. Using the orbital period, eccentricity, and pericenter argument given by the RV solution of Gaia DR3; adopting the effective temperature and radius of the companion obtained from SED; and setting that the companion's mass is $M_2 = 0.84M_\odot$ determined by single-star MIST evolutionary models, we fitted three controlling physical parameters of our light-curve model, which are the binary inclination (i), the isotropic irradiating luminosity of the suspected pulsar ($L_{\rm irr}$), and a phase shift. We adopt uniform priors of [17.°4, 29.°8] for the binary inclination, which correspond to the pulsar mass ranging from $1.17M_\odot$ to $3.00M_\odot$. The last parameter can account for any small offsets that might be present between the phase-folded light curves and the models, which further calibrate for the epoch of the time of periastron passage.

With the built-in optimizer demcmc of the ELC code, we searched for the best-fit solution by minimizing the χ^2 value, and the least reduced chi-square of $\chi^2_\nu = 4.2$. The best-fit ELC model along with the TESS photometry are shown in Figure 7. From the best-fit model, we obtain the binary inclination ($i = 27.^\circ 9$) and the isotropic irradiating luminosity ($L_{\rm irr} = 5.0 \times 10^{34}\,{\rm erg \cdot s^{-1}}$). Utilizing the binary mass-function $f(M) \sim 0.049M_\odot$ and the companion mass $M_2 = 0.84M_\odot$, the pulsar mass is $M_{\rm NS} \sim 1.30M_\odot$. The characteristic "isotropic irradiating luminosity" $L_{\rm irr}$ is related to the pulsar's spin-down luminosity, $L_{\rm sd}$, as $\eta L_{\rm sd} = L_{\rm irr}$. We can obtain the pulsar's spin-down luminosity, $L_{\rm sd} \sim 1.6 \times 10^{35}\,{\rm erg \cdot s^{-1}}$, by assuming the heating efficiency η is 0.3 (Breton et al. 2013; Li et al. 2014),

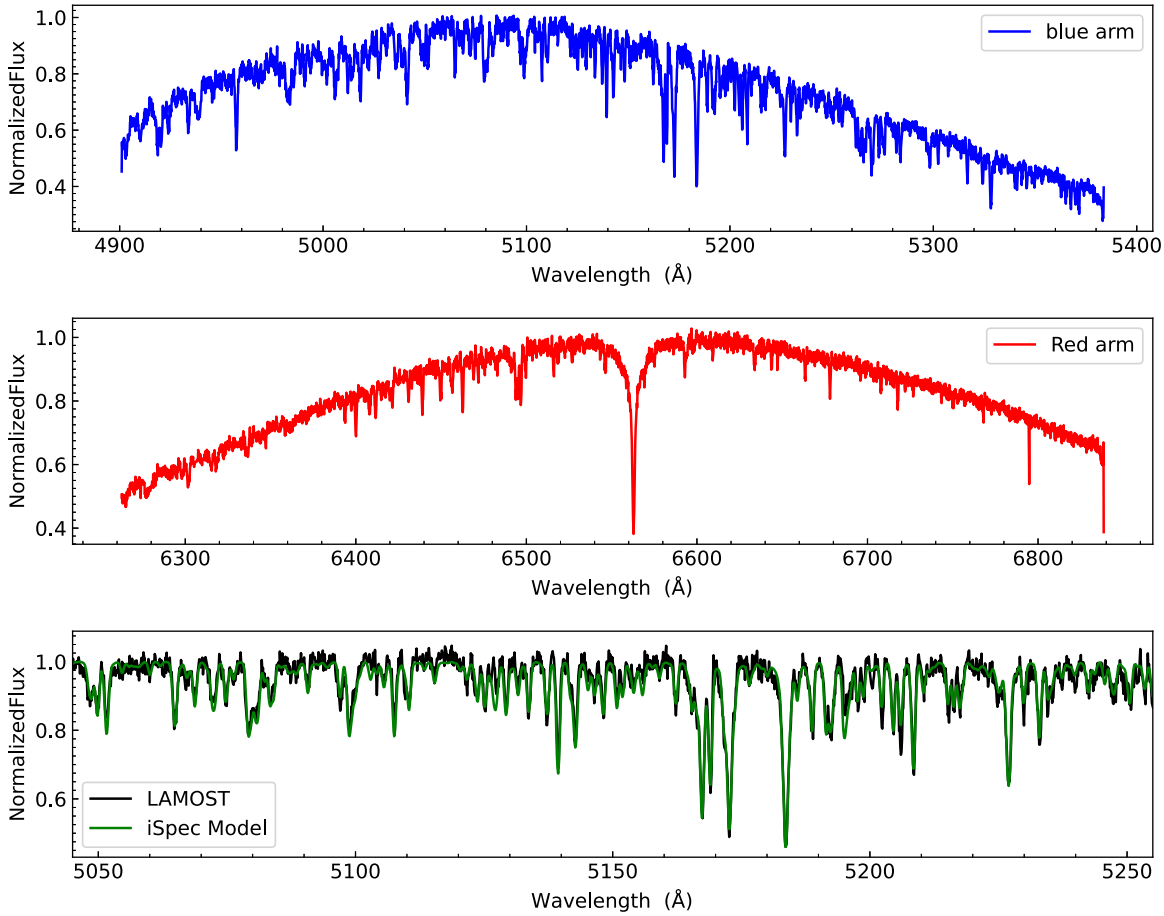

Figure 6. Top: the mid-resolution LAMOST spectra of the blue arms are shown. Middle: the mid-resolution LAMOST spectra of the red arms are shown. Bottom: a model spectrum in the blue arms using the atmospheric parameters derived from iSpec is shown in green.

which is considered typical for energetic MSPs ($L_{\rm sd} \sim 10^{34-35}{\rm erg \cdot s^{-1}}$). The spin-down luminosity of the pulsar is much larger than the intrinsic luminosity of the companion star, which may lead to strong ablation of the companion star. We note that it is not a good fit statistically due to a large χ^2_ν, also seen from the fit residuals, which likely related to asymmetric heating or starspots on the companion (Romani & Sanchez 2016; van Staden & Antoniadis 2016; Sanchez & Romani 2017).

3. Discussion

3.1. Asymmetric Light Curves

In addition, we note that the heating light curve is sometime asymmetric and shows evidence of flaring, which resembles similar behavior of XMMU J083850.38-282756.8 and PSR J1048 + 2339 in the optical (Halpern et al. 2017; Cho et al. 2018). The unusual asymmetric light curves are also observed in other redback MSPs, such as PSR J1628–3205 and a candidate redback MSP 3FGL J2039–5618 (Li et al. 2014; Salvetti et al. 2015). So far, there is no obvious origin of this asymmetry. Possibilities include an intrabinary shock distorted by orbital motion or direct channeling of the pulsar wind by a magnetic field intrinsic to the companion star or companion stellar activity (Tang et al. 2014; Romani & Sanchez 2016; van Staden & Antoniadis 2016; Halpern et al. 2017; Sanchez & Romani 2017). However, the results of the Lomb–Scargle periodogram for different epochs may suggest the presence of starspots. Therefore, the starspots may be mainly responsible for the often seen irregular and asymmetric light curves.

3.2. Formation and Evolution of 4FGL J1318.2+6754

The binary orbital period of 4FGL J1318.2+6754 is highly unusual among the compact binary MSPs if its redback nature is confirmed, challenging the standard recycling scenario where a neutron star is spun up to MSPs via accretion of mass and angular momentum from a companion star in an LMXB (Alpar et al. 1982; Tauris et al. 2012). A small filling factor poses serious problems for the standard recycling scenario.

Regarding the formation of this system, there are two possibilities. Following King et al. (2003) and King et al. (2005), the system's formation requires two stages. First, a binary MSP with a He WD companion is produced through the evolution of an LMXB. Second, by an exchange encounter event, the He WD is replaced by a main-sequence star. When the emission from the pulsar heats up the companion star, the system evolves into a redback system. In this case, the binary system can be eccentric and detached. However, considering that 4FGL J1318.2+6754 is located in the galactic field and there is a low stellar density, the probability of this scenario is low.

On the other hand, this system can be directly produced from an AIC of an oxygen–neon–magnesium (ONeMg) WD in a binary system (Freire & Tauris 2014; Smedley et al. 2015). In this scenario, an ONeMg WD accretes material from its

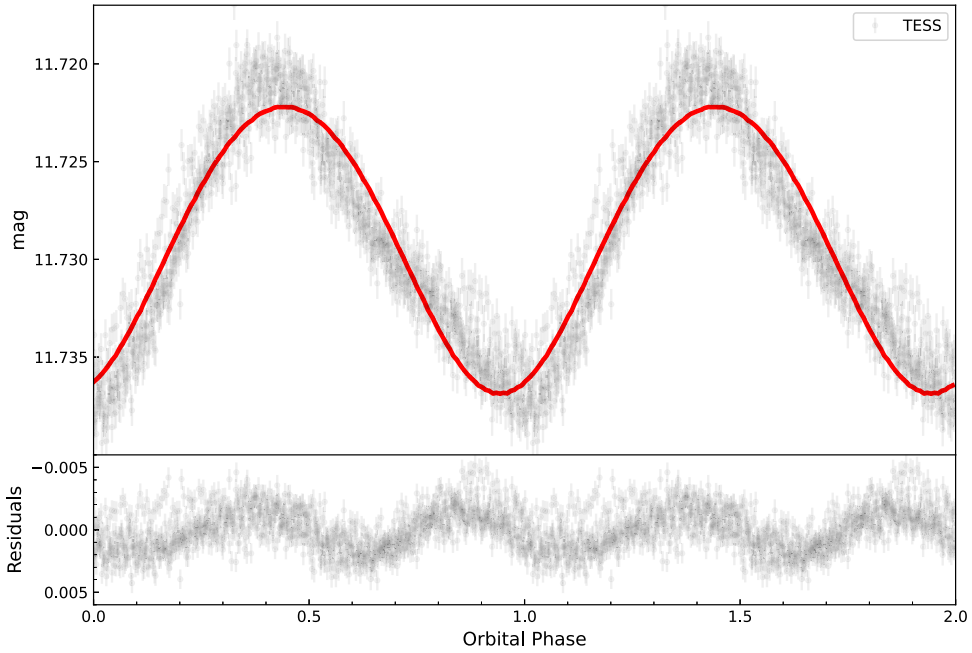

Figure 7. TESS optical photometry of J1318 in 2019 August. The red lines show the best-fit ELC code model. Bottom panel shows residuals for the difference between the observed and calculated magnitudes.

companion until its mass is reaches the Chandrasekhar-mass limit ($M_{\rm Ch} = 1.38 M_{\odot}$; Ablimit 2019). Then the WD directly collapses into an MSP.[9] Due to the mass loss during the AIC and natal kick of the NS, the binary system will become eccentric and binary separation becomes larger, leading to the detachment of the system (Tauris et al. 2013). Subsequently, the relativistic pulsar wind interacts with the companion to heat its photosphere and help drive a wind. We suggest that 4FGL J1318.2+6754 is likely to be at this phase. Assuming the AIC is a symmetric implosion with a negligible momentum kick and the pre-AIC binary orbit is circular, the sudden release of gravitational binding energy imposes an eccentricity to the system given by Bhattacharya & van den Heuvel (1991) $e = (M_{\rm Ch} - M_{\rm NS})/(M_{\rm NS} + M_2) \sim 0.04$, where $M_{\rm NS} = 1.30 M_{\odot}$ and $M_2 = 0.84 M_{\odot}$ are the mass of an MSP and companion, respectively. Given that the natal kick is small, the eccentricity should be small even if the natal kick is considered. This eccentricity is consistent with the RV solutions of Gaia DR3.

In addition, one may expect that binary pulsars formed via AIC have much smaller systemic velocities (10–30 $\rm km s^{-1}$) compared with those NSs formed via core-collapse supernovae (Tauris et al. 2013). Here, the system has a small proper motion (μ) of $\sim$7.72 mas $\rm yr^{-1}$ reported by Gaia, which gives a transverse velocity of $V_{\rm t} = 4.74 \mu D$ km $\rm s^{-1} \sim 14.63$ km $\rm s^{-1}$ (Lyne & Lorimer 1994). Combining the center-of-mass velocity from the RV solution of Gaia DR3, one can obtain the system's space velocities of $\sim$20.92 km $\rm s^{-1}$(Tauris et al. 2013), which is consistent with the properties of the AIC channel. Therefore, we propose the long-period redback candidate may be directly formed via AIC of a WD during the evolution of a WD–main sequence (MS) binary.

The subsequent evolution of the system is rather uncertain, since the influence of the emission of the pulsar on the companion is still very unclear. Here, we can only provide a very broad and general discussion. If the fraction of pulsar emission energy used to ablate the companion star is relatively large, the binary separation may become larger and larger as the mass of the companion star becomes smaller and smaller (Smedley et al. 2015). Eventually this system may evolve into an isolated MSP, but if the fraction of pulsar emission energy used to ablate the companion star is very small, the system may evolve into an LMXB as the companion star fills its Roche lobe and the radio signal of the NS is suppressed. In this case, this system will evolve into a binary MSP with He WD companion eventually.

[9] During this process, if the WD is spun up to rapid rotation, the WD may avoid collapse when its mass reaches the Chandrasekhar-mass limit. After the end of the mass transfer, the WD is spun down and collapses into an NS. This is referred to as delayed AIC. Here, we did not consider the effect of rotation.

4. Conclusions

We found an SB1 inside the 95% error ellipse of 4FGL J1318.2+6754 and speculated that it is a redback MSP binary. In the TESS observation, it has a variable heating light curve similar to those observed of redback pulsars with irradiation of the companion star by an MSP. This further supports that it is a redback MSP binary. In addition, although the system has a small mass-function, $f(M) \sim 0.049 M_{\odot}$, the light curve of low amplitude implies the system has a small inclination angle to favor a redback MSP binary. The asymmetric heating light curve can be interpreted as the production of an intrabinary shock distorted by the orbital motion or the magnetic field channeling pulsar wind particles and radiation directly onto the surface of the main-sequence star. Using the LAMOST RVs, we validate the orbital solution of Gaia DR3 for the system. We also searched for periodicity in the TESS data and found the peak at the period $P = 4.137258763046017$ days, which is compatible with the Gaia SB1 solution. This orbital period of $P \sim 4.13$ days corresponds to the longest orbital period for known redback candidates and confirmed systems in Galactic globular clusters. More importantly, the redback MSP binary of a 4.13 day orbit period could hardly form under the standard recycling scenario. Based on its small proper motion, we

propose that the redback MSP binary may be produced via an AIC event of ONeMg WD in a WD–MS binary.

Acknowledgments

We appreciate the anonymous referee for the constructive suggestions and comment. We also think Dr. Kejia Lee for his helpful comments and suggestions. The Guoshoujing Telescope (the Large Sky Area Multi-Object Fiber Spectroscopic Telescope, LAMOST) is a National Major Scientific Project built by the Chinese Academy of Sciences. Funding for the project has been provided by the National Development and Reform Commission. LAMOST is operated and managed by the National Astronomical Observatories, Chinese Academy of Sciences. This Letter includes data collected with the TESS mission, obtained from the MAST data archive at the Space Telescope Science Institute (STScI). Funding for the TESS mission is provided by the NASA Explorer Program. STScI is operated by the Association of Universities for Research in Astronomy, Inc., under NASA contract NAS 5-26555. This research has made use of the SIMBAD database, operated at CDS, Strasbourg, France. This work was supported by the National SKA Program of China (2020SKA0120100), the Strategic Priority Research Program of the Chinese Academy of Sciences, grant No. XDB0550300, the National Key R&D Program of China (grant No. 2021YFA1600403) and the CAS light of West China Program.

ORCID iDs

Jie Lin https://orcid.org/0000-0001-6311-6391
Renxin Xu https://orcid.org/0000-0002-9042-3044

References

Alpar, M. A., Cheng, A. F., Ruderman, M. A., et al. 1982, Natur, 300, 728
Abdollahi, S., Acero, F., Baldini, L., et al. 2022, ApJS, 260, 53
Ablimit, I. 2019, ApJ, 881, 72
Archibald, A. M., Stairs, I. H., Ransom, S. M., et al. 2009, Sci, 324, 1411
Benvenuto, O. G., De Vito, M. A., & Horvath, J. E. 2014, ApJL, 786, L7
Bhattacharya, D., & van den Heuvel, E. P. J. 1991, PhR, 203, 1
Blanco-Cuaresma, S. 2019, MNRAS, 486, 2075
Blanco-Cuaresma, S., Soubiran, C., Heiter, U., et al. 2014, A&A, 569, A111
Bogdanov, S., Archibald, A. M., Hessels, J. W. T., et al. 2011, ApJ, 742, 97
Breton, R. P., van Kerkwijk, M. H., Roberts, M. S. E., et al. 2013, ApJ, 769, 108
Burdge, K. B., Marsh, T. R., Fuller, J., et al. 2022, Natur, 605, 41
Chen, H.-L., Chen, X., Tauris, T. M., et al. 2013, ApJ, 775, 27
Cho, P. B., Halpern, J. P., & Bogdanov, S. 2018, ApJ, 866, 71
Choi, J., Dotter, A., Conroy, C., et al. 2016, ApJ, 823, 102
Cui, X.-Q., Zhao, Y.-H., Chu, Y.-Q., et al. 2012, RAA, 12, 1197
Dotter, A. 2016, ApJS, 222, 8
Freire, P. C. C., & Tauris, T. M. 2014, MNRAS, 438, L86
Gaia Collaboration 2022, VizieR Online Data Catalog, Gaia DR3 Part 1. Main source
Gaia Collaboration, Arenou, F., Babusiaux, C., et al. 2023, A&A, 674, A34
Gentile, P. A., Roberts, M. S. E., McLaughlin, M. A., et al. 2014, ApJ, 783, 69
Gray, R. O., & Corbally, C. J. 1994, AJ, 107, 742
Green, G. M., Schlafly, E., Zucker, C., et al. 2019, ApJ, 887, 93
Gustafsson, B., Edvardsson, B., Eriksson, K., et al. 2008, A&A, 486, 951
Halpern, J. P., Strader, J., & Li, M. 2017, ApJ, 844, 150
King, A. R., Beer, M. E., Rolfe, D. J., Schenker, K., & Skipp, J. M. 2005, MNRAS, 358, 1501
King, A. R., Davies, M. B., & Beer, M. E. 2003, MNRAS, 345, 678
Kong, A. K. H., Huang, R. H. H., Cheng, K. S., et al. 2012, ApJL, 747, L3
Li, M., Halpern, J. P., & Thorstensen, J. R. 2014, ApJ, 795, 115
Lin, J., Li, C., Wang, W., et al. 2023, ApJL, 944, L4
Lomb, N. R. 1976, Ap&SS, 39, 447
Lyne, A. G., & Lorimer, D. R. 1994, Natur, 369, 127
Orosz, J. A., & Hauschildt, P. H. 2000, A&A, 364, 265
Papitto, A., Ferrigno, C., Bozzo, E., et al. 2013, Natur, 501, 517
Price-Whelan, A. M., Hogg, D. W., Foreman-Mackey, D., et al. 2017, ApJ, 837, 20
Roberts, M. S. E. 2013, in IAU Symp. 291, Neutron Stars and Pulsars: Challenges and Opportunities After 80 Years (Cambridge: Cambridge Univ. Press), 127
Romani, R. W., Kandel, D., Filippenko, A. V., et al. 2022, ApJL, 934, L17
Romani, R. W., & Sanchez, N. 2016, ApJ, 828, 7
Romani, R. W., & Shaw, M. S. 2011, ApJL, 743, L26
Salvetti, D., Mignani, R. P., De Luca, A., et al. 2015, ApJ, 814, 88
Sanchez, N., & Romani, R. W. 2017, ApJ, 845, 42
Scargle, J. D. 1982, ApJ, 263, 835
Smedley, S. L., Tout, C. A., Ferrario, L., et al. 2015, MNRAS, 446, 2540
Tang, S., Kaplan, D. L., Phinney, E. S., et al. 2014, ApJL, 791, L5
Tauris, T. M., Langer, N., & Kramer, M. 2012, MNRAS, 425, 1601
Tauris, T. M., Sanyal, D., Yoon, S.-C., et al. 2013, A&A, 558, A39
van Staden, A. D., & Antoniadis, J. 2016, ApJL, 833, L12
Vines, J. I., & Jenkins, J. S. 2022, MNRAS, 513, 2719
Yi, T., Gu, W.-M., Zhang, Z.-X., et al. 2022, NatAs, 6, 1203
Yuan, H., Wang, S., Bai, Z., et al. 2022, ApJ, 940, 165
Zheng, L.-L., Sun, M., Gu, W.-M., et al. 2023, SCPMA, 66, 129512
Zong, W., Fu, J.-N., De Cat, P., et al. 2020, ApJS, 251, 15